Seasonal microclimate control of calcite fabrics, stable isotopes and trace elements in modern speleothem from St Michaels Cave, Gibraltar

David P. Mattey, Ian J. Fairchild, Tim C. Atkinson, Jean-Paul Latin, Mark Ainsworth and Richard Durell

Geological Society, London, Special Publications 2010; v. 336; p. 323-344
doi:10.1144/SP336.17

Seasonal microclimate control of calcite fabrics, stable isotopes and trace elements in modern speleothem from St Michaels Cave, Gibraltar

DAVID P. MATTEY[1,*], IAN J. FAIRCHILD[2], TIM C. ATKINSON[3], JEAN-PAUL LATIN[4], MARK AINSWORTH[4] & RICHARD DURELL[4]

[1]*Department of Earth Sciences, Royal Holloway University of London, TW20 0EX, UK*

[2]*School of Geography, Earth & Environmental Sciences, University of Birmingham B15 2TT, UK*

[3]*Department of Earth Sciences, University College London, WC1E 6BT, UK*

[4]*Cliffs and Caves Section, Gibraltar Ornithological and Natural History Society, Gibraltar*

**Corresponding author (e-mail: mattey@es.rhul.ac.uk)*

Abstract: Detailed monitoring of three drip sites in New St Michael's Cave, Gibraltar, reveals a strongly coherent seasonal pattern of dripwater chemistry despite each site having significantly different flow paths and discharge patterns. Calcite saturation is closely linked to regular seasonal variations in cave air pCO_2 caused by seasonally reversing ventilation driven by temperature difference between the cave interior and the air outside. A coupled model of CO_2 degassing and calcite precipitation links seasonal $\delta^{13}C$ variations in coexisting dripwater, cave air CO_2 and speleothem calcite to large variations in pCO_2 that are driven by cave ventilation. The relationships between stable isotope ratios, Sr/Ca and speleothem fabrics across annually formed calcite laminae are consistent with a degassing–calcite precipitation process in which rapid degassing controls the $\delta^{13}C$ of both drip water DIC and calcite whereas a much slower rate of calcite precipitation causes seasonal cycles of Sr in a more complex manner. By demonstrating the causes of laminated speleothem fabrics plus trace element and isotope cycles in modern speleothem from a closely monitored cave, this study provides clear links between the local microclimate and the proxy record provided by speleothem geochemistry. In Gibraltar, low cave air pCO_2 in summer is unusual compared to what has been revealed by cave monitoring carried out elsewhere and shows that caution is needed when linking paired speleothem fabrics to specific seasons without knowledge of local processes operating in the cave.

Speleothems provide continuous and precisely dated records of past environmental change which have advanced understanding of climate variability on timescales from glacial–interglacial cycles (Wang *et al.* 2008) down to seasonal patterns of precipitation (Borsato *et al.* 2007). Speleothem deposition in stable cave environments can record changes in surface climate as variations in properties such as extension rate, trace element abundances and stable isotopes (McDermott 2004; Fairchild *et al.* 2006*a*) but the causal relationships between these proxies and climate are not always fully understood. For some proxies they appear to be straightforward, for example the dependence of extension rate on the amount of rainfall (Baker *et al.* 2008), but for others such as stable isotopes interpretations have often been based on assumptions and guesswork regarding the aspects of climate that are most closely reflected. Ideally, any proxy-climate transfer function used should be based on a full understanding of the physico-chemical workings of the local climate–karst-cave system and its influences on the recording process.

Careful, multi-annual monitoring of the cave microclimate, dripwater chemistry and calcite growth mechanisms reveals some of the local effects that may modify the climate recording process. Some of the important issues include the relationships between precipitation, recharge, drip rates and solute chemistry (Bottrell & Atkinson 1991; Genty & Deflandre 1998; Baker & Brunsdon 2003; Tooth & Fairchild 2003; Cruz *et al.* 2005; Baldini *et al.* 2006; Genty 2008), the role of seasonal ventilation and degassing (Ek & Gewelt 1985; Bar-Matthews *et al.* 1996; Spötl *et al.* 2005; Banner *et al.* 2007; Baldini *et al.* 2008) and the impact of kinetic factors such as fast degassing or crystal chemical effects on $CaCO_3$ growth (Hendy 1971; Mickler *et al.* 2004, 2006). Knowledge of these local processes and their stability through time are a critical step in the derivation of reliable climate–proxy transfer functions that can be used for quantitative climate reconstruction.

From: PEDLEY, H. M. & ROGERSON, M. (eds) *Tufas and Speleothems: Unravelling the Microbial and Physical Controls*. Geological Society, London, Special Publications, **336**, 323–344.
DOI: 10.1144/SP336.17 0305-8719/10/$15.00

Several recent studies of speleothem records at high resolutions have revealed climate features on seasonal (Treble *et al.* 2003; Johnson *et al.* 2006; Banner *et al.* 2007; Mattey *et al.* 2008) or even synoptic time scales (Frappier *et al.* 2002) which provide the critical direct link between the local weather and how it is recorded during the speleothem deposition process. Speleothem calcite deposition in caves is commonly seen to be cyclical, resulting in the development of laminae defined by alternating pairs of fabrics (Baker *et al.* 2008; Genty & Quinif 1996). Using constraints from growth on dated artefacts and ^{14}C analyses (Baldini *et al.* 2005; Genty *et al.* 2001; Tan *et al.* 2006; Mattey *et al.* 2008) cyclic laminae have sometimes been shown to be annual features and related to strong seasonality of the local climate. Annual growth laminae provide a means of deriving a chronology at the best possible precision, and may also preserve trace element and stable isotope patterns that can be related to the local climate and hydrological cycle.

Our work in Gibraltar combines comprehensive multi-annual cave monitoring with high resolution analyses of fabric, trace elements and stable isotopes in modern speleothem. A recent study of a modern stalagmite from New St. Michaels Cave (Mattey *et al.* 2008) revealed annual growth laminae which preserve exceptionally well-defined seasonal $\delta^{13}C$ and $\delta^{18}O$ cycles linked to ventilation. We were able to identify the $\delta^{18}O$ of winter dripwater from the complex seasonally resolved speleothem record and show excellent inter-annual correspondence with the $\delta^{18}O$ of winter precipitation. In the present paper we present a more detailed overview of the results of the first 4 years of cave environment monitoring which includes local meteorology, cave and soil temperature, humidity and pCO_2, and of drip discharge and monthly analysis of drip water for trace element and isotopic analysis. The monitoring data enable the seasonally resolved speleothem fabric, trace element and isotope record to be precisely linked to the nature and timing of local processes in the soil, cave air and local climate. We propose a coupled CO_2 degassing–calcite precipitation model which links the development of annual cycles in $\delta^{13}C$ and Sr with the effects of seasonal cave ventilation.

Regional setting, monitoring techniques and analytical methods

Old and New St Michaels Caves

The Rock of Gibraltar, located where the Atlantic meets the Mediterranean at the junction of Europe and Africa, forms a North–South trending ridge 2.5 km long with a maximum elevation of 423 m (Fig. 1). The ridge is asymmetric, having a steep to near-vertical eastern slope which is partly banked by Pleistocene sand-dune deposits, and a western slope falling more steadily at 35° towards the town of Gibraltar near sea level. Above 100 m altitude the western slopes are covered in Mediterranean scrub forest with low rock outcrops of the Gibraltar limestone. The peninsula of Gibraltar links the Betic and Rif mountain chains, which form the southwestern end of the Mediterranean Alpine belt and is mainly composed of early Jurassic age limestone and dolomite which form the lower limb of an overturned nappe (Rose & Rosenbaum 1991). These beds dip steeply to the west and although there are no surface streams, swallets or resurgence features, the dolomites and limestones contain many solution caves located at altitudes ranging from below present sea level to near the summit ridge at over 400 m. Many caves have natural entrances exposed by erosion, but other significant caves have also been revealed though tunneling (Rosenbaum & Rose 1991).

The location and a plan of St Michaels Cave is shown on Figures 1 and 2. Old St Michaels Cave (OSM) (Shaw 1955) has been known since Roman times and is open to tourists as a show cave. The cave has developed in faulted dolomitic limestone creating a large main chamber. Dissolution has also followed bedding planes, creating minor caves linked to OSM and forming natural entrances to the system. During World War II, a new access tunnel was driven into the lowest part of the show cave, known as the Hospital, exposing a lower series of solution rifts leading southwards along the strike of the Gibraltar limestone at an altitude of around 325 m (Fig. 2). This system, New St Michaels Cave (NSM) (Shaw 1954), rivals the old show cave system in terms of the scale of speleothem decoration, and also contains a 6 m deep lake which accumulates water from seepages and drips entering the southern part of NSM.

Gibraltar caves such as the St Michaels system preserve evidence of phreatic origins and have since undergone several phases of draining and decoration with secondary speleothem deposits (Tratman 1971). Because the present altitude of the large St Michaels system is over 300 m asl, the phreatic features indicate that these caves have undergone significant uplift to their present position (Tratman 1971; Rose & Rosenbaum 1991; Rodrigues-Vidal *et al.* 2004). Tunnelling near sea level in the 19th century revealed more large natural caves such as the Ragged Staff system with similar overall morphology but with far less speleothem deposition. Ragged Staff Cave contains brackish lakes with water filled passages extending

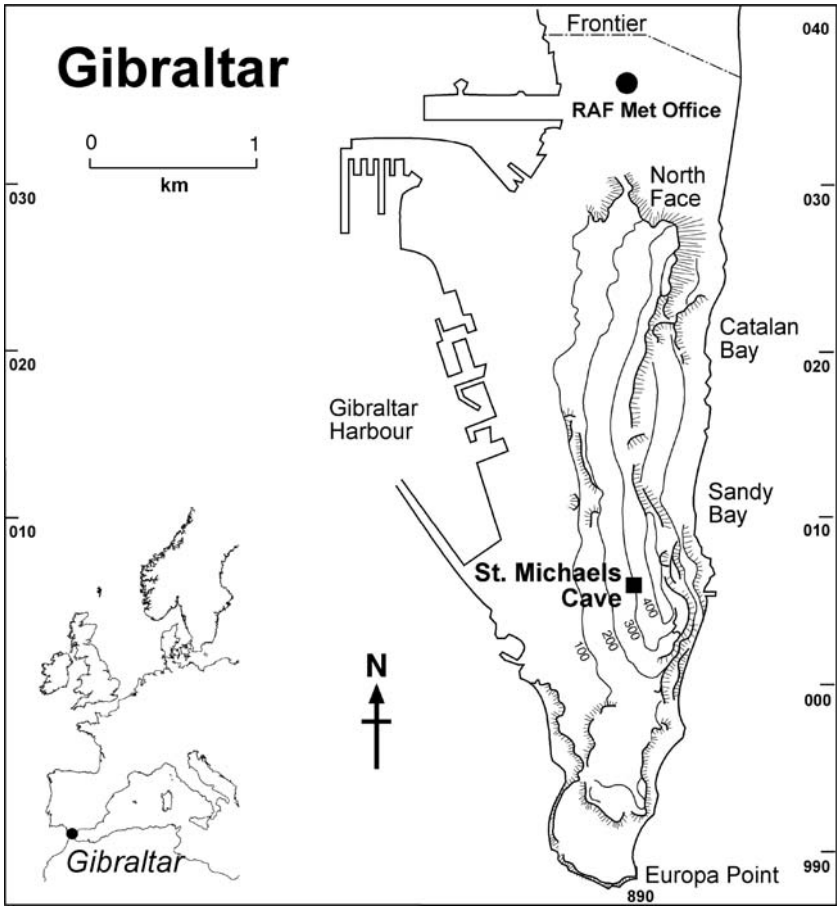

Fig. 1. Location of Gibraltar, St. Michaels cave and other features described in the text. Figure adapted from Mattey *et al.* (2008).

below sea level suggesting that initial phases of dissolution may have taken place by mixing near the freshwater-seawater interface via processes similar to flank margin cave formation (Mylroie & Carew 1988; Romanov & Dreybrodt 2006). Wave-cut platforms (90 and 130 m asl) are a prominent feature of the geomorphology of Gibraltar (Rodriguez-Vidal *et al.* 2004) recording higher stands of sea level in the past, and although the age and development history of Gibraltar caves are not yet well understood, solution voids and their subsequent decoration by speleothem deposition may be controlled by neotectonic uplift in conjunction with sea level fluctuations between glacial and interglacial periods (Rodriguez-Vidal *et al.* 2004).

OSM has a number of natural entrances as well as artificial high and low level tunnels used for tourist access. The showcave develops strong natural chimney ventilation (Wigley & Brown 1976; Atkinson *et al.* 1983) between high- and low-level entrances and is known to show seasonal reversals in flow direction. In winter, warm cave air flows upwards drawing cool outside air into the lower entrances whereas in summer cave air flows out of lower entrances, drawing atmosphere into upper entrances. Before modern development for tourism the natural entrances would all have been at a higher level and chimney ventilation may not have been as strong a feature as it is at the present time. The NSM cave system has no known natural entrances and remained unconnected to OSM until the link was made in 1942 with the lowest part of main show cavern. Seasonally reversing chimney ventilation can also be detected though the 1 m^2 trapdoor link between OSM and NSM, although sealing this connection for one month in August 2006 was found

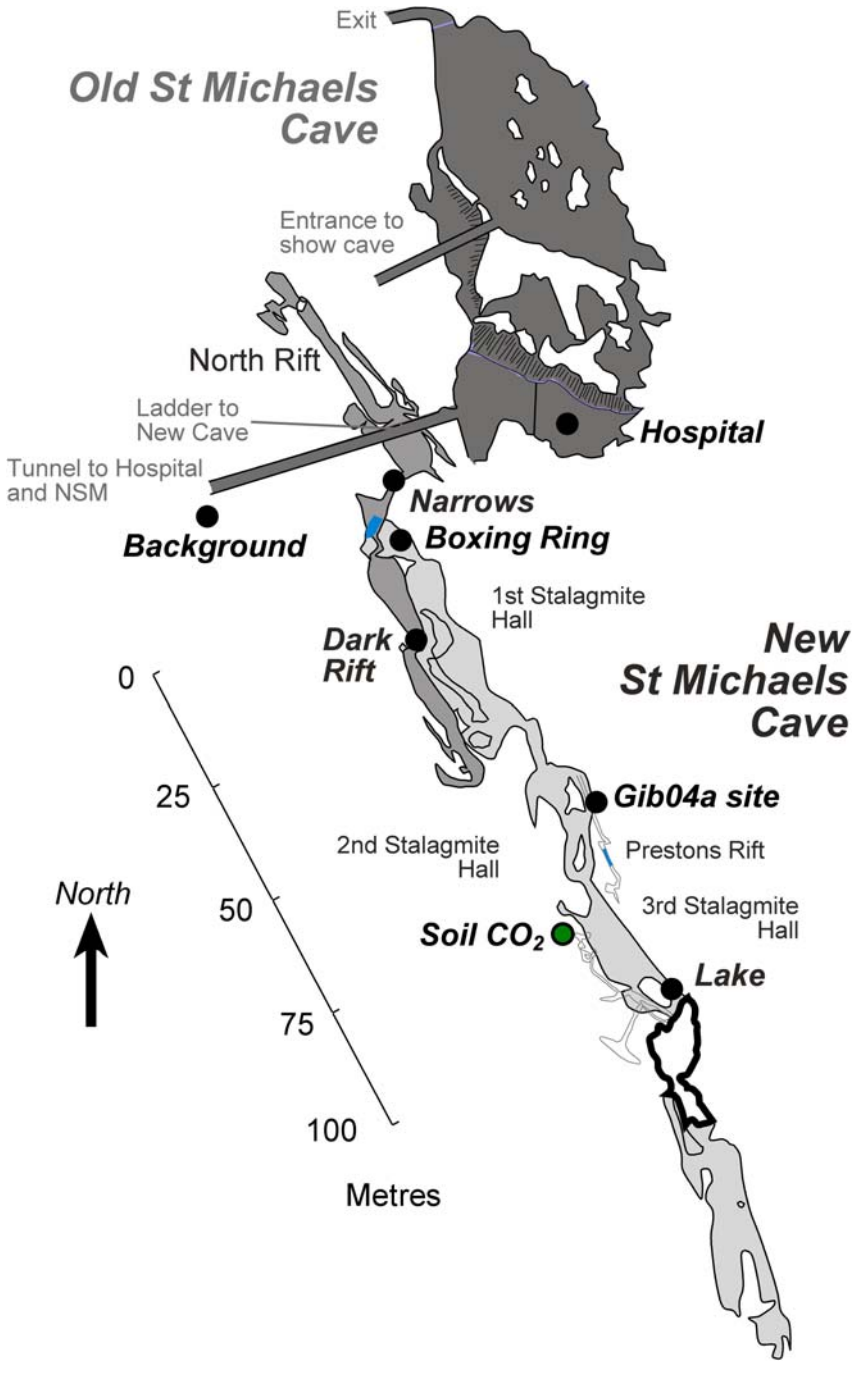

Fig. 2. Plan of the St. Michaels Cave systems based on the survey by Shaw (1954) and figures from Rose & Rosenbaum (1991). Locations of monitoring sites and features discussed in the text are shown.

to have no impact on CO_2 levels and ventilation of NSM as a whole (our unpublished data). Deeper within the NSM system very weak air flow patterns can be detected using smoke tracers, but the dramatic seasonal fluctuations in CO_2 levels described by Mattey *et al.* 2008 and in

this work suggest the existence of connections to the surface or other caves which allows large-scale natural advective transport of air through the entire system.

Cave environmental monitoring

All meteorological data were recorded at the RAF Meteorological Office located 3 km away from the cave (Fig. 1). The cave monitoring, sampling and analysis program obtained data via continuous logging (l) and spot measurements or sample(s) taken during regular monthly visits from June 2004–April 2008, for the following parameters:

1. cave air: pressure (l), temperature (l) and relative humidity (l,s), mixing ratios of CO_2 (l,s) and CH_4 (s), analysis of $\delta^{13}C_{CO2}$ and $\delta^{13}C_{CH4}$ (s)
2. soil: temperature (l) and soil air mixing ratios of CO_2 and CH_4 (s), analysis of $\delta^{13}C_{CO2}$ and $\delta^{13}C_{CH4}$ (s)
3. drip water: discharge (l); pH, total alkalinity, electrical conductivity, cations, $\delta^{18}O$ and δD (s)

The locations of environmental monitoring sites are shown on the cave plan in Figure 2. Seasonal variations in temperature and relative humidity in ambient air at the cave entrance, within the main chambers of the cave system and within the soil zone above the cave (temperature only) were measured by continuous logging supplemented by spot measurements made using hand held instruments during monthly visits. Temperature and humidity were measured by continuous logging using single- (temperature) and dual-channel (temperature and humidity) loggers from Gemini Data loggers deployed outside above the cave entrance tunnel, and in the Hospital, Dark Rift and Gib04a sites within the cave (Fig. 2). Soil temperature at 50 cm depth was logged at the soil CO_2 sampling site (see below). Temperature-logging at a resolution of 0.4 °C early in the project was improved to 0.1 °C resolution at some sites from 2007. Spot measurements were made at the time of sampling at air and drip water sampling sites and all temperature measurements were corrected relative to a BS certified mercury thermometer to an accuracy of ± 0.05 °C.

Surveying and dye tracing

A line survey was carried out to accurately position the map of NSM made by Shaw (1954) relative to surface topography. This showed that the soil monitoring site is located almost directly over the cave (Fig. 2) and allowed us to identify sites for injecting dyes with the aim of tracing connections between infiltrating rainwater and points where seepage enters the cave. Following methodology described by Smart (1976) and Bottrell & Atkinson (1992), two aliquots of the fluorescent dye Photine CU were simultaneously released into excavated fissures in bedrock at nearby points above the Gib04a site in the cave. A second dye, Diphenyl Brilliant Flavine DY96, was washed into scree at a third point at a higher altitude, located where the dip of the Gibraltar limestone projected upwards from Gibo4a in the cave intersects the surface near the summit ridge (Fig. 3). The injections were made in March 2007 during a period of high rainfall, and the dyes were washed into the ground by runoff from sheets of polythene placed for this purpose. Within the cave, a network of cotton detectors were deployed at 27 stations. These provided regular monitoring for both tracers for 85 days after the date of injection, as well as a period of background monitoring for 59 days beforehand.

Drip water discharge rates, sampling and analysis

Drip water was collected in a HDPE beaker containing an acoustic drip rate logger (Collister & Mattey 2008) and fitted with an outlet tube leading to a 1.5 l storage reservoir open to cave air. The drip logger counted the total drips falling in 30 minute intervals and counts were converted to discharge in l/d based on a mean drop volume of 0.15 ml (Collister & Mattey 2008) for all sites.

Aliquots of water were stored in 100 ml HDPE doubly sealed bottles and pH, conductivity and alkalinity were measured within two hours of sampling. pH was determined using a Jenway pH and conductivity probe which was calibrated at pH 7 and 10 before the sampling session. Alkalinity was determined on site by titration against bromocresol green using a Hach digital titrator. Dripwater cation analyses were determined by ICP-AES in the Department of Earth Sciences, Royal Holloway with a total precision of less than 5%. All isotopic analyses in this study were carried out using GV Instruments Multiflow–Isoprime systems at Royal Holloway. Drip water $\delta^{13}C$ DIC was determined by acidification of 0.5 ml of water with orthophosphoric acid and equilibrating for 7 h at 40 °C. $\delta^{13}C$ values were normalized to the V-PDB scale via a calibrated sodium bicarbonate internal standard and have an external reproducibility of better than 0.08‰.

Air sampling and analysis

Spot samples of background atmosphere, cave air and soil gas were collected in 1 l or 3 l Tedlar

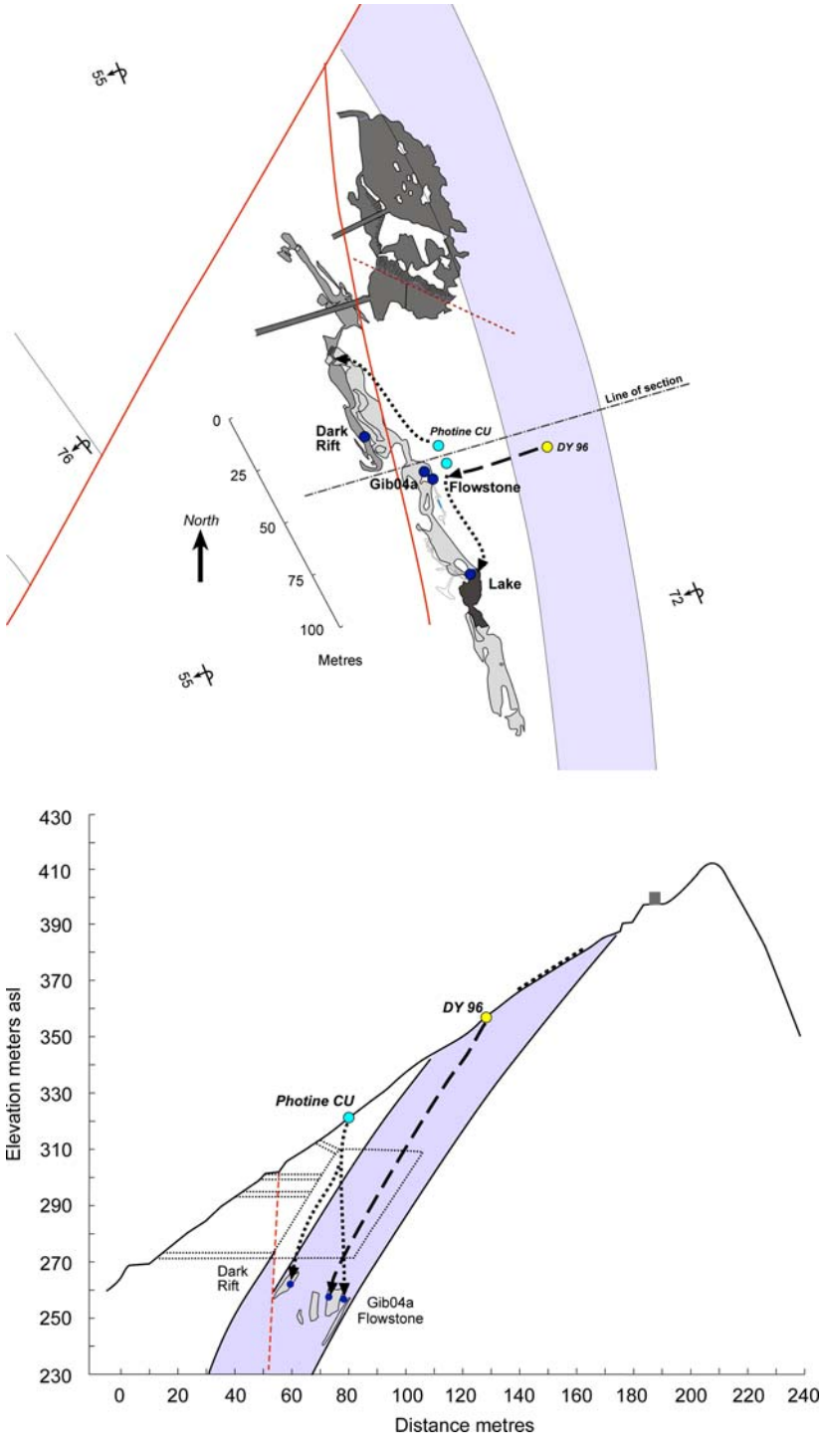

Fig. 3. Geological setting of St. Michaels Cave showing injection sites for the yellow dye DY96 (yellow) and blue dye Photine CU (blue) together with schematic flow pathways. Bedrock geology adapted from the map compiled by Rosenbaum & Rose (1991). Cave plan located relative to 1000 m UTM grid co-ordinates using data from a new line survey carried out in 2007.

bags using a small hand-held pump for analysis of mixing ratios and the $\delta^{13}C$ of CO_2. Soil gas samples were collected initially using a steel tube inserted into the soil and from June 2007 using porous PTFE gas sampling cells permanently buried at 25 cm and 50 cm depth. Mixing-ratio analysis of CO_2 was carried out using a LiCor 6252 NDIR analyser calibrated against NOAA standards. Isotope analyses of CO_2 were determined using a GV Instruments Trace Gas – Isoprime system and precisions (1σ) for 10 consecutive analyses of the secondary standard tank were between 0.03–0.05‰ for carbon dioxide $\delta^{13}C$ analysis.

Results

Cave temperature and humidity

The variation of temperature and humidity within the OSM and NSM cave systems generally decrease as a function of distance from entrances, and temperatures approach the local mean annual values in the deeper parts of NSM. In detail, though, these variations are quite complex both in terms of spatial position within the cave, and as a function of the time of year. Variations in cave air temperature and humidity at two of the monitoring sites, the Hospital (the lowest part of the show cave, Fig. 2) and at the GIb04a site (representative of the distal areas of the NSM system, Fig. 2) measured by continuous logging and monthly using hand held instruments are summarized in Figure 4. Figure 4a compares three NSM cave air temperatures measured in 1948, 1954 and 1958 (Shaw 1955; Tratman 1971), the mean annual temperature (MAT) at the cave entrance measured in this study between 2004–2008 and the local MAT recorded by the Meteorological Office since 1940. The MAT plotted on Figure 4 are sea level data corrected to the corresponding temperature at 325 m asl using a lapse rate calculated from over 1300 measurements of the difference in mean daily temperature measured at the Hospital tunnel entrance (Fig. 2) and at sea level by the Meteorological Office station (1.22 ± 0.25 °C). The three historic spot measurements show a 1.6 °C range and cannot be distinguished from modern temperatures which are within error of the MAT corrected for altitude. Unfortunately there are insufficient data to assess whether cave temperatures tracked the decreasing and then rising trend in MAT observed since 1948 (Fig. 4).

Temperatures monitored by continuous logging appear to be relatively constant in the deep cave ($< \pm 0.4$ °C) but show marked seasonal variation of around 3 °C in the Hospital area of the show cave (Fig. 4c, d). Relative humidity measurements average $95 \pm 3\%$ in the deep cave but are again are much more variable in the Hospital area (Fig. 4b). Here temperatures are significantly lower than the MAT of 17.5 °C all year round and fail to reach MAT even by the end of the summer (Fig. 4d). Humidity in the Hospital area is also lowest in winter when chimney ventilation is vigorously pulling cold outside air through the show cave (Fig. 4b). The permanently below-MAT temperatures of the showcave indicate that winter ventilation removes sufficient heat from cave wall rock such that the mean annual temperature of the Hospital area (16.3 °C) remains over 1 °C cooler than the annual outside MAT (17.5 °C) (cf. Atkinson *et al.* 1983). Conversely, the slightly higher MAT of the deeper NSM (17.9 °C) may be indicative of advected warmer air rising from lower levels in the rock, a hypothesis developed in more detail below to explain the cave air CO_2 data.

Spot measurements taken over the four-year period are more variable than data returned by temperature logging recording spot measurements at 30-minute intervals and suggest that there may some local short term variation of up to ± 0.5 °C at the Gib04a and other deeper sites in NSM. Although the 0.4 °C resolution of the early logging devices would not have fully resolved such small variations in air temperature, logging since June 2008 at an improved 0.1 °C resolution fails to record regular seasonality (Fig. 4) indicating that small fluctuations in air temperature may occur even in the more distal regions of OSM and are too rapid to be clearly resolved by temperature loggers recording at 30-minute intervals.

Drip-rate variations and recharge pathways

Following the release of tracers near the end of the period of winter recharge Photine CU was detected at sites dispersed along the length of the cave (Fig. 3). The drip falling onto the Gib04a stalagmite itself was not monitored but the Photine dye was detected at seepages nearby. The position of the two Photine injection sites almost directly above the cave requires that the detected dye must have followed a nearly vertical pathway through 68 m of rock to reach these. Dye was also detected in seepages up to 60 m horizontally NW of the nearest injection, and 50 m away S–SE. These pathways have overall deviations of 41° and 36° from vertical, and indicate that percolation through a network of interlinked voids spread the tracer laterally between paths that diverge vertically by up to 77°. The second dye, DY96, was detected at the flowstone site, which lies almost directly down dip from the injection point (Fig. 3). This dye was found at only a few of the other sites monitored, and the fluorescence at these was much weaker and less prolonged than at the flowstone site.

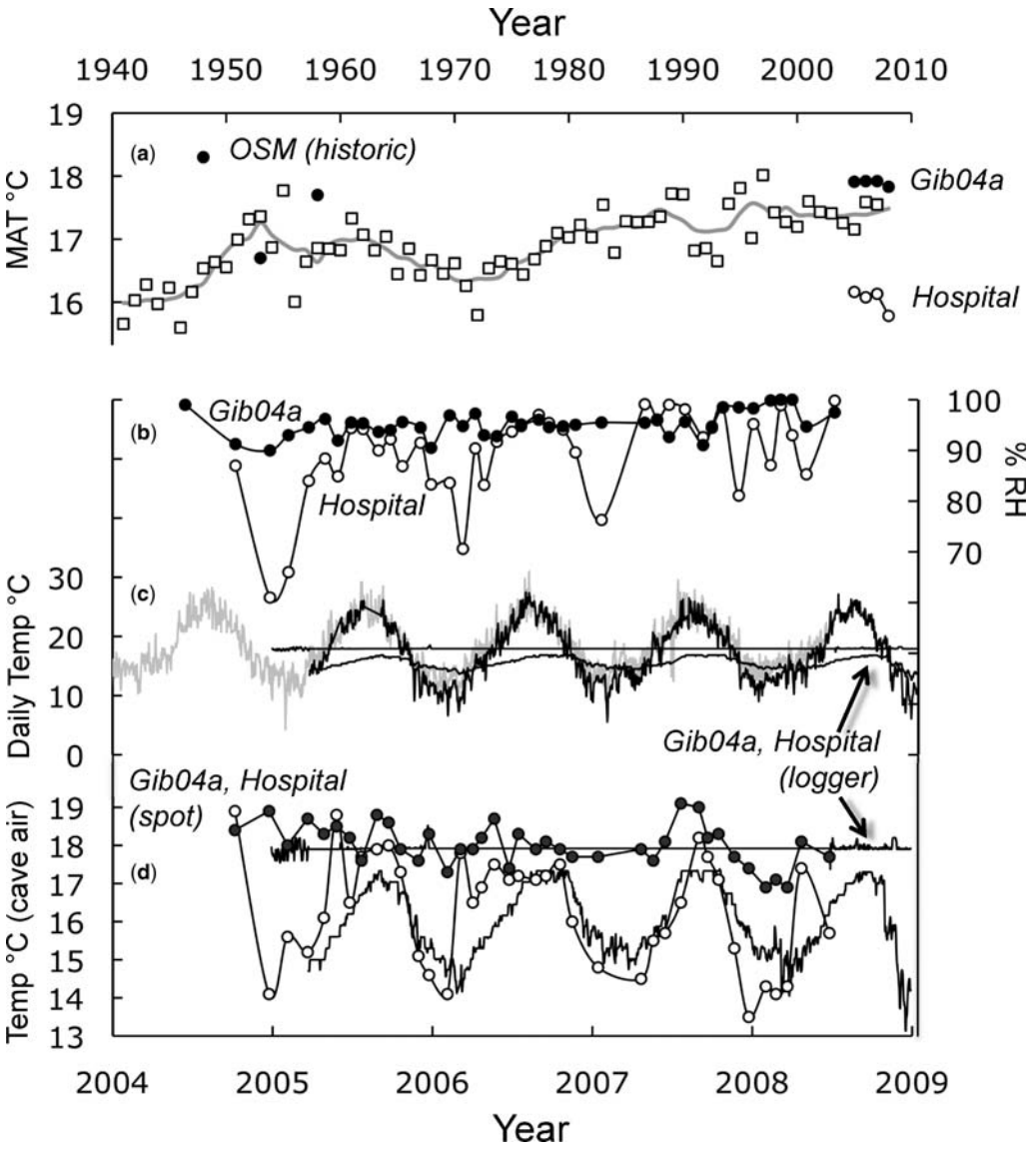

Fig. 4. Temperature and humidity variations from 2004–2009. (**a**) Mean annual temperatures (MAT) at the airport (open squares), adjusted by 1.22 °C to be comparable with the cave data as described in the text, compared with historic OSM spot data and MAT from logging at cave sites Gib04a (closed circles) and Hospital (open circles). (**b**) spot relative humidity measurements at the Gib04a and Hospital sites. (**c**) Comparison of daily mean temperature measurements measured at seal level by the Met Office (grey) and at the cave entrance (black) with daily average cave air temperatures measured at the Hospital (weak seasonality) and Gib04a sites (flat line). (**d**) Spot temperature measurements compared with logged temperatures at the Gib04a and Hospital sites. The Hospital site displays much larger variations than Gib04a, which lies deeper in the cave interior. Meteorological data © The Met Office, UK.

However these subsidiary detections were spread along the length of the cave, indicating that percolation of the DY96 took place along a principal channel feeding the flowstone site, but was also spread laterally through a network of subsidiary channels. The horizontal angle across which this spread occurred was 70°, which is similar to the vertical angle of spread displayed by the Photine tracer. The angle between vertical and the pathway to the flowstone site is 30°. Taking the patterns of

detection of the two dyes together, it seems probable that infiltrating waters follow bedding-parallel fractures for distances up to *c*. 100 m, but also migrate vertically down intersecting joints and small faults. The properties of the 3-D network of fractures are such that each dye probably spreads through a volume shaped approximately as an upright half-cone with its apex at the point of injection, its axis vertical, and the vertical plane of bisection of the apical angle lying parallel to the strike of the limestone beds. The half-angle at the apex of this cone is about 35°. Such strong lateral dispersion of the tracers implies that infiltrating water derived from any single point on the surface must mix extensively with water from other points. However the fact that DY96 was detected strongly at only one site indicates that some parts of the flow network are effectively channeled parallel to the bedding and that these channeled pathways encounter relatively few distributary junctions. Such pathways may be expected to show less mixing, and seepages fed by them may therefore possess distinctive chemistry and/or hydrological characteristics compared with others that are derived from better mixed parts of the network. Such contrasts do in fact occur between the three seepage sites that were monitored as part of this work.

Variations in drip discharge rates at three sites measured at 30-minute intervals across three annual hydrological cycles are shown in Figure 5 and show that drip responses to the seasonal pattern of winter rain differ dramatically at each site. The Gib04a speleothem site (Mattey *et al.* 2008) is fed at a low discharge of 0.04 to 0.06 l/d which shows no direct relationship to the winter–summer cycle of recharge or to individual high-rainfall events. Dye-tracing suggests it is fed by mixed water from a recharge zone that lies upslope and directly above the cave chamber where the roof thickness is 64 m (Fig. 3). The drip rate pattern is consistent with flow through roof rock which has a capacity for significant storage and mixing before emerging at the drip site.

The drip monitoring site in the Dark Rift, situated at a higher level in the cave system (Fig. 2) shows a more complex drip response that is highly correlated with periods of heavy rainfall. The enlarged scale in Figure 5 shows that the drip rate has a base flow component of a similar magnitude to that seen at a lower level at the Gib04a site, but this is punctuated by short-lived but intense discharge events which may peak at over 8 l/d for a few hours. At the beginning of the winter season there is a six-hour lag between the start of a rainfall event and the sharp rise in drip rate which subsequently declines usually to a new, higher level of base flow. The sharp response may be termed quick-flow and is suggestive of a channeled pathway. Each winter season begins with a high degree of correlation between rain and quick-flow events but as the wet season develops this relationship becomes less clear, presumably as recharge fills the fracture network and flow switching begins to contribute water from other reservoirs. Neither dye was detected at this site, but Photine CU was found at two drips a few metres away, suggesting that the the main recharge zone for base flow lies directly above the cave chamber where the roof thickness is around 38 m. Analogy with the spread of DY96 tracer suggests that the recharge for the quick-flow component may lie somewhat upslope and feed the same reservoir as the baseflow. The pattern of water chemistry at this site suggests a source that is quite distinct from both Gib04a and the flowstone site.

The flowstone site is located at the same level and less than 4 m away from the Gib04a site (Fig. 3). Here the drip response shows remarkable annual regularity with peak discharges around mid-January exceeding 80 l/d. The discharge rate then steadily declines for the remaining winter season and by the start of the following autumn the site is close to drying up. In winter 2005/6 the flowstone discharge ceased completely until mid-January but during 2006/7 and 2007/8, although flows increased erratically at the start of the winter rainfall season, the peak discharge was delivered in each case at the same time in mid-January. Dye-tracing reveals that this water is fed from a recharge zone near the summit of the Rock, and groundwater follows bedding places down to the flowstone site. The unusual cyclical pattern of delayed peak discharge followed by an exponential decline suggests the operation of a siphon which carries over accumulated early winter rainfall into a second reservoir that directly feeds the flowstone. During heavy periods of rainfall the siphon can be by-passed creating irregular pulses observed before the main discharge event in January. Water reaches this site via a longer flow path (*c*. 120 m) and the drip water, whose composition is also quite different with higher levels of Ca and total alkalinity (see below), is depositing flowstone on the cave floor.

Cave water hydrochemistry

The main features of compositional variation in cave waters are illustrated in Figures 6 and 7. The Mg/Ca compositions of lake and drip water are compared on Figure 6a and show coherent trends consistent with extensive prior calcite precipitation (PCP) from parental waters having Ca values at or above the upper limits of the water analyzed (Fairchild *et al.* 2000). The rationale for this is that calcites have much lower Mg/Ca than the waters

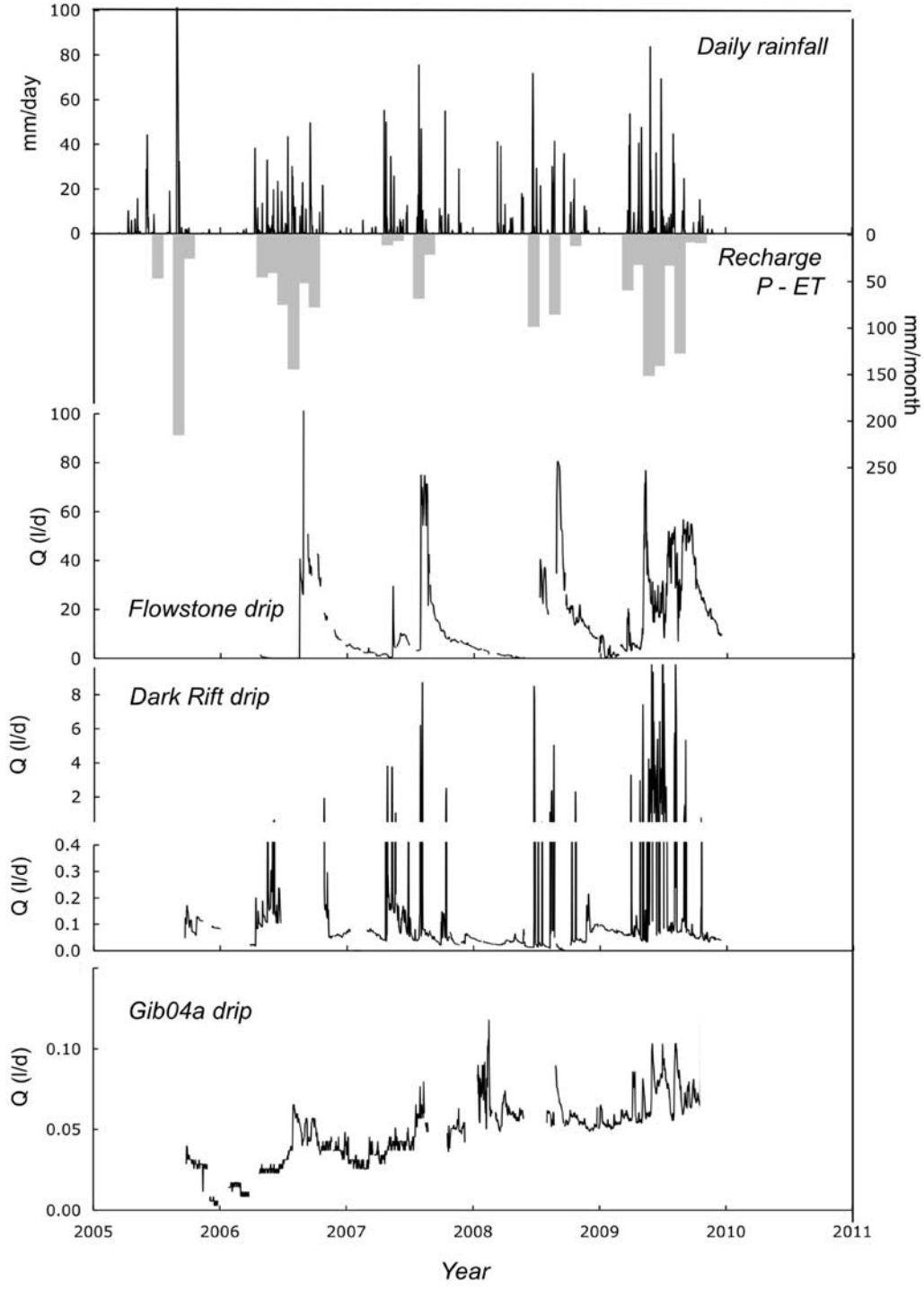

Fig. 5. Comparison of drip discharge rates at the Flowstone, Dark Rift and Gib04a sites compared with daily rainfall and recharge expressed as monthly P-ET. Daily water discharge rates were calculated using data from continuously logged using acoustic drip counters and a drop volume of 0.15 ml (Collister & Mattey 2008). Daily rainfall amounts were measured at the Gibraltar Meteorological Office, 3 km from the entrance to St. Michaels Cave and P-ET calculated using the Thornthwaite method (Thornthwaite 1948). Meteorological data © The Met Office, UK.

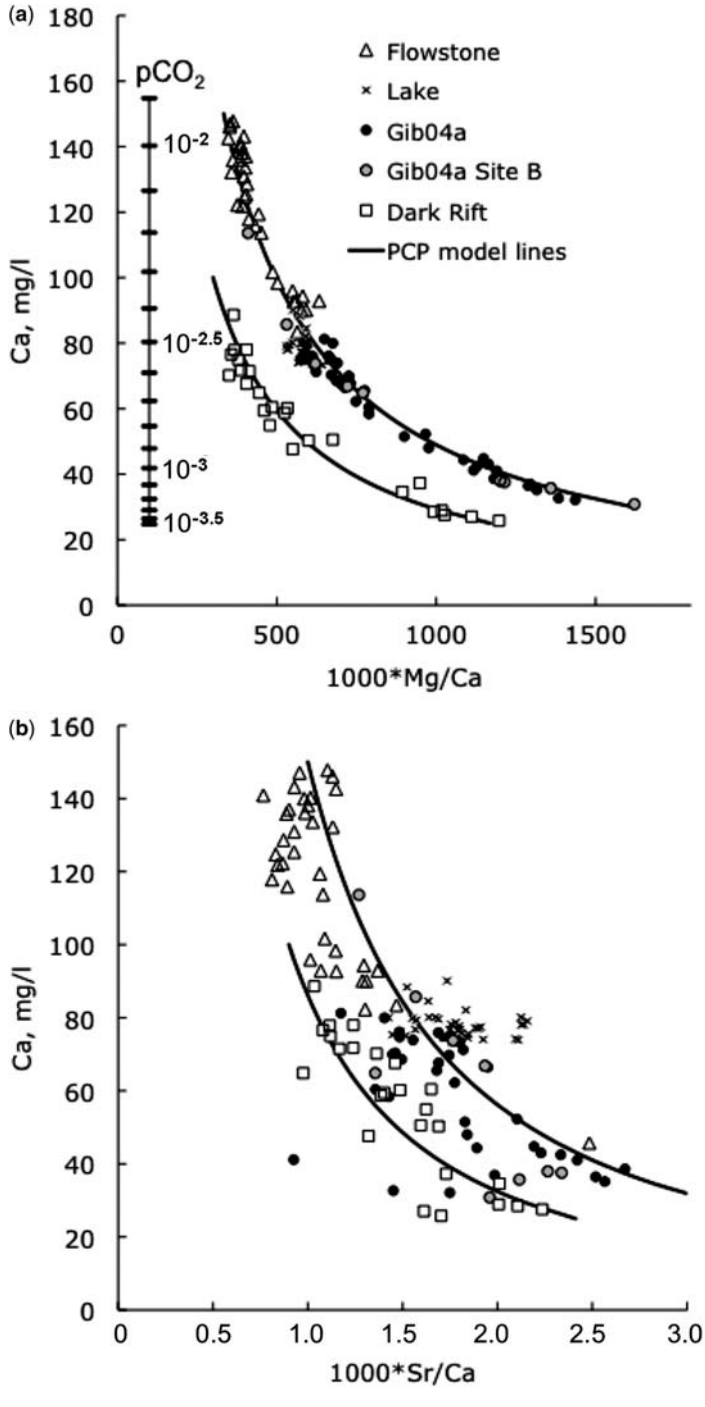

Fig. 6. (**a**) Plot of Ca versus Mg/Ca ratios for NSM waters compared with modeled prior calcite precipitation (PCP) lines. The distribution coefficient for Mg in calcite (K_{Mg}) used for modeling is 0.02, but the lines are not sensitive to the exact value. The pCO_2 values correspond to those at equilibrium with calcite for waters of appropriate Mg/Ca using MIX4 modeling (Fairchild *et al.* 2000). (**b**) Similar plot for Sr/Ca; value of K_{Sr} used is 0.3 (Huang & Fairchild 2001). See text for discussion.

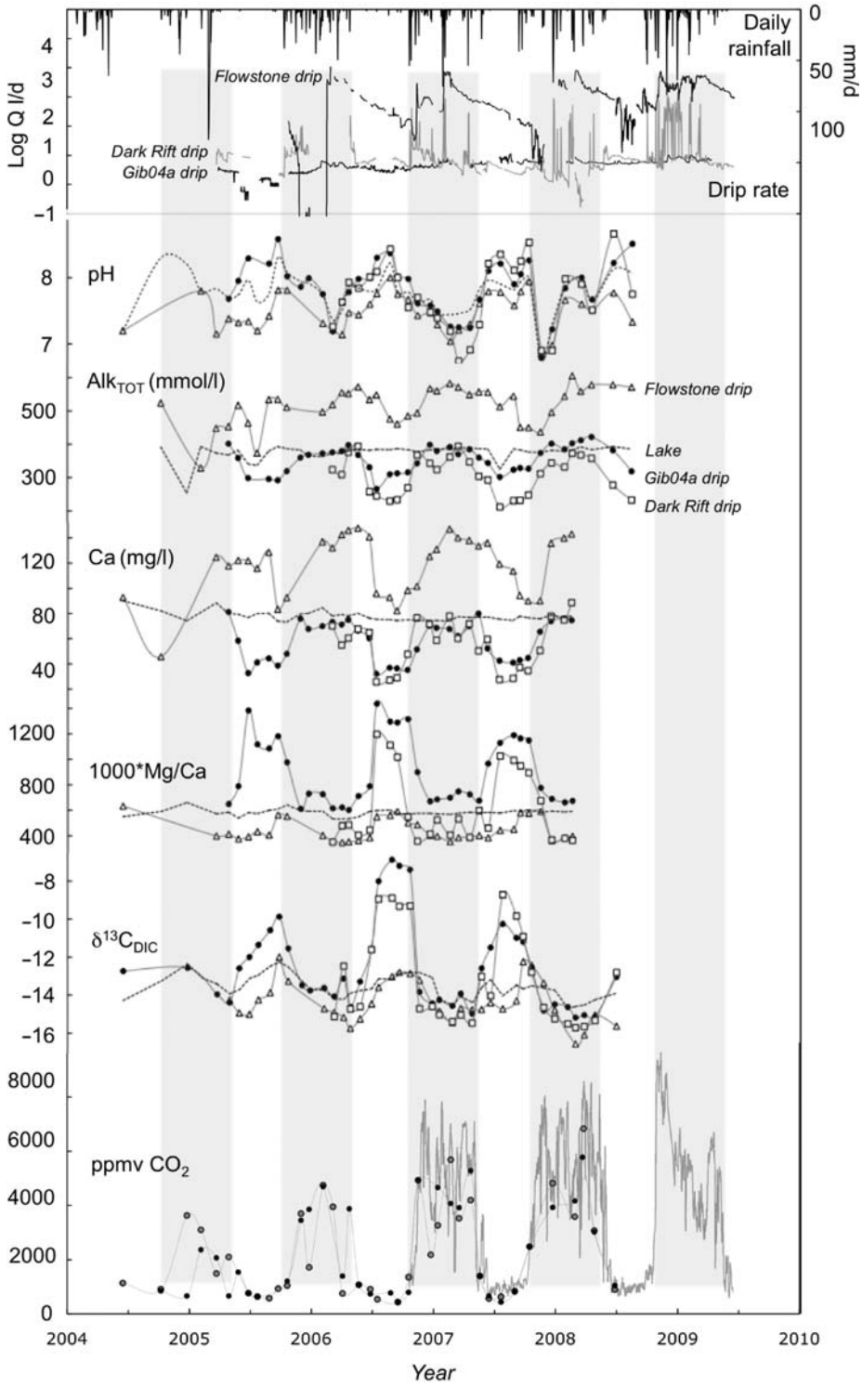
Daily rainfall
mm/d
Log Q l/d
Flowstone drip
Dark Rift drip
Gib04a drip
Drip rate
pH
Alk$_{TOT}$ (mmol/l)
Flowstone drip
Lake
Gib04a drip
Dark Rift drip
Ca (mg/l)
1000*Mg/Ca
$\delta^{13}C_{DIC}$
ppmv CO_2
Year

Fig. 7.

from which they form such that the distribution coefficient (K) is small:

$$K_{Mg} = (Mg/Ca)_{water}/(Mg/Ca)_{calcite} = 0.02 \quad \text{(at 17 °C; Huang \& Fairchild 2001)} \qquad (1)$$

Hence as calcite is precipitated along the flowline, Ca changes much more than Mg and drip water compositions evolve following curves on Figure 6 such as the two PCP model lines illustrated. The highest-Ca waters along a trendline represent waters that are least modified and their pCO_2 value constrains the minimum value encountered by the waters along their flow route. The highest-Ca points are those that feed the flowstone, which has a recharge zone at a higher altitude and is delivered to the drip site along bedding planes via a siphon. The Ca concentrations reach over 140 mg/l Ca, corresponding to equilibrium at a pCO_2 of $>10^{-1}$ ($\approx$ 7% CO_2 by volume), and since the cave air has a much lower pCO_2 values, degassing leads to a high degree of supersaturation and vigorous precipitation of calcite as flowstone. Lake water samples collected monthly over the monitoring period are generally more constant in composition relative to drip water in terms of Ca (around 80 mg/l) and with initial Mg/Ca ratios similar to drip water from the Gib04a site (Fig. 6a). The Gib04a drip water shows a large seasonal decrease in Ca to below 40 mg/l accompanied by a shift in Mg/Ca to >1500 as a result of seasonal calcite precipitation during the summer months (Fig. 7).

Drip waters from the Dark Rift are offset from the other data samples. Although this could reflect a source with a lower ratio of dolomite to calcite, it is notable that the lowest Mg/Ca ratios are very similar for the Dark Rift waters and the flowstone waters and both may represent the original composition of bedrock being dissolved. These minimum 1000*Mg/Ca values are around 400, corresponding to a molar Mg/Ca ratio of around 1/3 suggesting dissolution of 2/3 dolomite and 1/3 limestone. Note that the proportion of limestone bedrock would be expected to be much lower than this because of faster calcite dissolution (Fairchild *et al.* 2000). The reason for the lower Ca values of the Dark Rift could be that its water acquires its dissolved CO_2 from soil air rather than the more CO_2-rich source from which Gib04a is evidently derived. Soil air has lower pCO_2 values (no more than $10^{-1.4}$ ($\approx$ 4% by volume) according to Fig. 6a) and indeed variability in soil pCO_2 is expected from its highly varied thickness and moisture content.

Figure 6b illustrates Sr data which also illustrate the PCP effects. These data are more scattered at each site which is probably at least partly analytical because of the very low Sr concentrations (typically 0.1 ppm) encountered. There is a less marked increase in Sr/Ca as Ca falls compared with Figure 6a. This is due to a relatively high value for K_{Sr} (a value of 0.3 was used to construct the lines in Figure 6b; Huang & Fairchild 2001).

Figure 7 shows monthly variations of cave water pH, total alkalinity, Ca, Mg/Ca, and $\delta^{13}C_{DIC}$, in relation to drip discharge and cave air CO_2 levels from late 2004 to late 2008/early 2009. An obvious feature of the data is the strong seasonal pattern of variation where drip water collected in winter months has lower pH, highest total alkalinity, highest Ca, lowest Mg/Ca, and lowest $\delta^{13}C_{DIC}$. Another striking feature is the coherent pattern of variation displayed by water collected at drip sites which are each significantly different from each other in terms of flow paths (Fig. 3) and discharge patterns (Fig. 4). The flow stone drip water has a distinctive composition having higher Ca and total alkalinity levels yet shows the same seasonal patterns of variation; the lake water reservoir also displays similar, but more attenuated seasonal variations in hydrochemistry. This commonality in seasonal behaviour suggests a common control that must be located *within the cave*, because it affects waters with such diverse hydrology and chemistry.

Cave air CO_2 and ventilation regimes

CO_2 mixing ratios in cave air sampled monthly from NSM at the GIb04a sites and from the lake area are shown on the lowest graph in Figure 7. As for the temperature and humidity variations discussed above, the distribution of cave air CO_2 also shows complex patterns of spatial as well as strong temporal variation which are clearly related to regular diurnal and seasonal cycles modified by local synoptic scale weather conditions. Overall, cave air CO_2 mixing ratios show very regular seasonal variations with highest concentrations in winter

Fig. 7. (*Continued*) Relationships between rainfall amount, drip discharge, dripwater composition and cave air pCO_2 measured between 2004–2009. Grey bands mark the period between mid-November and mid-April when cave air pCO_2 is highest. From top to bottom: daily rainfall; drip discharge rates from Figure 5 plotted together on a log scale; monthly dripwater pH, total alkalinity, Ca concentration, 1000*Mg/Ca and $\delta^{13}C_{DIC}$. Lower plot is the concentration of CO_2 in deep cave air, measured on monthly spot samples at the Gib04a (black circles) and Lake (grey circles) sites along with data (unpublished) obtained by continuous logging at 2 hr intervals measured at the Gib04a site. Meteorological data © The Met Office, UK.

(3000–6000 ppmv) falling to around 500 ppmv in the summer. Continuous monitoring of CO_2 levels at seven locations has been carried out since October 2006 and shows that CO_2 concentrations can exceed 10 000 ppmv for brief periods and are subject to rapid fluctuations which are closely related to wind strength and direction rather than barometric pressure (our unpublished data). These data also clearly show that the seasonal switch from high to low CO_2 modes is closely correlated with the temperature difference between the exterior and interior of the cave which seasonally reverses chimney ventilation driven by density contrast of cave air. Thus the high winter levels of CO_2 in cave air are diluted in the summer by penetration of outside atmosphere.

The switches between winter and summer modes take place in mid-April and mid-November and correspond to the external temperature respectively rising above and falling below the MAT of the deep cave (17.9 °C). The former allows dilution by the atmosphere and the latter permits CO_2 levels to rise by flux from the interior of the Rock. This chimney ventilation is clearly revealed by seasonal temperature and humidity variations in OSM, but ventilation dilution of CO_2 is observed in even the most distal regions of NSM despite having no known natural entrances and only linked to the show cave via a small hatchway. Furthermore, the transition from high winter levels to low summer levels is very rapid and occurs throughout the cave system within hours. Sealing of the hatchway between OSM and NSM for a month in August 2007 had no effect on the CO_2 behavior in NSM and dilution of cave air must take place via natural pathways to other caves or directly to the surface. These observations, supported by data for CH_4 and $\delta^{13}C$ data for both CO_2 (see below) and CH_4 (to be presented elsewhere), provide compelling evidence for seasonal advective transport of CO_2-rich 'ground air' through macroporous Gibraltar limestone via enlarged bedding planes and joints. Whether this process is local to the elevated cave systems located near the summit of the Rock or part of a larger scale advective system affecting cave systems at other levels in the rock is not yet known.

The carbon isotopic composition of cave and soil air CO_2 is shown on a Keeling plot of $1/CO_2$ versus $\delta^{13}C$ in Figure 8. The $\delta^{13}C$ of cave air CO_2 shows wide variation between $-10‰$ to $-23‰$ which is a result of mixing between local atmosphere ($\delta^{13}C = -9.6‰$) and an isotopically light CO_2-rich component, a processes also seen in Obir cave

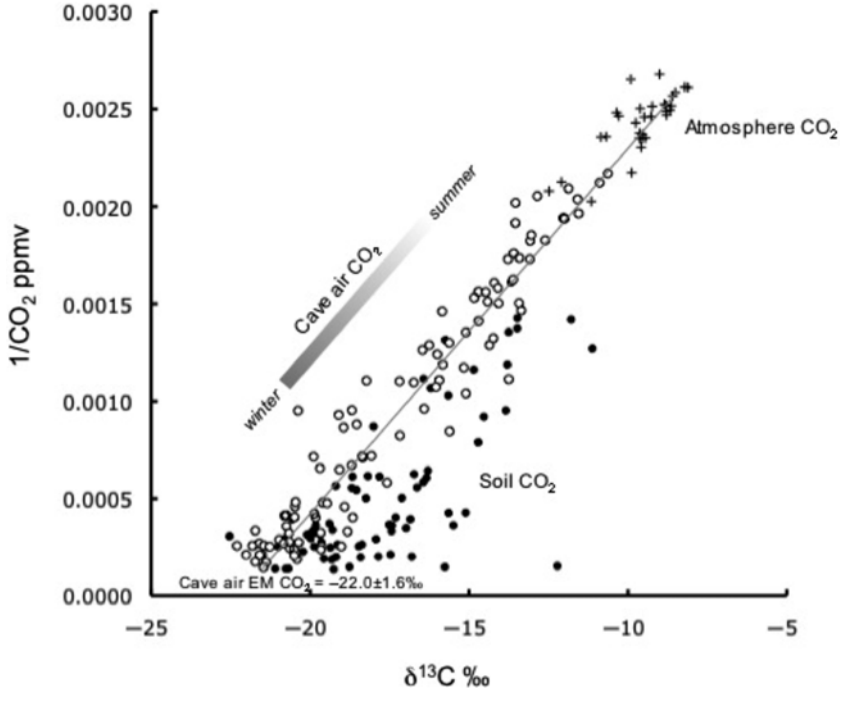

Fig. 8. Abundance and carbon isotopic composition of CO_2 in local atmosphere, cave air (all sites) and soil air. Line is a best fit mixing vector between atmospheric CO_2 and a 'ground air' CO_2 endmember with a $\delta^{13}C$ of $-22‰$. See text for discussion.

(Spötl *et al.* 2005). Sources of the CO_2-rich 'ground air' component may include CO_2 degassed from groundwater, CO_2 from the soil zone that has penetrated the epikarst as a gas phase, CO_2 respired from plant roots that may penetrate deeply into fractures, and CO_2 generated from decomposition of colloidal or dissolved organic matter in infiltrating water (Atkinson 1977; Wood & Petraitis 1984; Wood 1985). The tight mixing array on Figure 8 constrains the ground air $\delta^{13}C$ as $-22.0 \pm 1.5‰$ with no evidence of seasonal variation. Soil CO_2 levels measured from a site vertically above the cave (Fig. 2) show seasonal variation with lowest values in the dry summer months and maximum values reaching 7300 ppmv in the winter when soil moisture is greatest and bioproductivity is still active. The isotopic composition of soil air is shown on the Keeling plot on Figure 8 and forms a more scattered array that shown by cave air. The soil air CO_2 data are also a resulting of mixing, this time between a respired CO_2 end member and ambient atmospheric CO_2. The $\delta^{13}C$ of soil respired CO_2 is much more variable, ranging from -12 to $-22‰$ but does not show evidence of regular seasonality. The heavier values are most likely a result of diffusive loss of CO_2 to the atmosphere which is greatest during dry periods. Thus the lightest end member values approach the true value of respired soil CO_2 which, at $-20‰$ (Fig. 8), is slightly different (i.e. heavier) than the composition of CO_2-rich ground air inferred as the end-member of the mixed air observed in caves.

Calculated pCO_2 in equilibrium with undegassed cave drip waters ($>10^{-1}$ or 7% by volume, see above) are much higher than measured soil CO_2 concentrations and it is speculated that sites of karstic CO_2 production may lie below the soil zone in pockets where organic material has accumulated (cf. Atkinson 1977; Wood & Petraitis 1984; Wood 1985). In this environment CO_2 generation may take place at a more constant rate throughout the seasonal year to become the main source of 'ground air' percolating into the epikarst.

Discussion

Shifts in drip water chemistry may be a result of a variety of processes including changes in the water source composition, dilution of groundwater by rain, calcite precipitation elsewhere in the aquifer or changes in the degree of CO_2 degassing (Baldini *et al.* 2006; Banner *et al.* 2007; Spötl *et al.* 2005; Tooth & Fairchild 2003). In Gibraltar, the drip water compositions are largely independent of discharge rates and simultaneously have lowest pH (around 7) lowest $\delta^{13}C$ and highest Ca in winter and lowest Ca with highest pH and $\delta^{13}C$ DIC in summer. This seasonal variation is synchronized with changes in cave air CO_2 levels (Fig. 7) related to reversing chimney ventilation patterns. Covariance among non-conservative parameters such as pH, total alkalinity, $\delta^{13}C$, Mg/Ca and cave air pCO_2 are consistent with variable degrees of calcite precipitation coupled to CO_2 degassing which is externally controlled by the switch from winter 'high' to summer 'low' levels of cave air pCO_2. Modern speleothem carbonates forming in this environment are characterized by annual laminae composed of paired columnar and dark compact calcite bands which preserve well developed cycles in trace elements and stable isotopes (Mattey *et al.* 2008).

Evolution of calcite and drip water compositions in a seasonally ventilated cave

The composition and carbon isotopic evolution of drip water undergoing coupled degassing–calcite precipitation has been modeled as a Rayleigh fractionation process using PHREEQC and code adapted from Appelo & Postma (2007) in Figures 9a, b. The monthly compositions of coexisting cave air and drip water sampled between 2004 and 2009 are plotted on Figure 9a as cave air ppmv CO_2 versus $[Ca]_{drip\ water}$ and on Figure 9b as cave air ppmv CO_2 versus the $\delta^{13}C$ of cave air CO_2 and drip water HCO_3^-. Figure 9a also shows the curve for the compositions of solutions in equilibrium with calcite and CO_2(g) at 18 °C and curves showing the compositions of supersaturated solutions with calcite saturation indices (log of the ratio of ionic activity product to calcite solubility product) of 0.5, 1.0 and 1.5. Drip water compositions at both the flowstone and Gib04a sites define trends which are a result of variable amounts of coupled degassing–calcite precipitation from groundwater that is initially in equilibrium with water in very CO_2-rich environments. On emerging into ventilated cave spaces these waters are then subjected to degassing cycles driven by the winter–summer switches in cave air CO_2 levels. The flowstone drip waters carry the highest solute load (Figs 6 & 7) and the elevated Ca levels require that the groundwater originally equilibrated with carbonate in a very CO_2-rich environment where pCO_2 was in the order of 7% (Fig. 9a). This far exceeds the observed CO_2 levels in the soil zone suggesting that the site of CO_2 accumulation may be deeper, perhaps within voids along the inclined bedding planes forming the feeder network for the drip (Fig. 3). The Gib04a drip water, fed vertically downwards, equilibrated in an environment with a maximum pCO_2 of around 1% which is closer to the actual measured pCO_2 levels in the soil zone directly above.

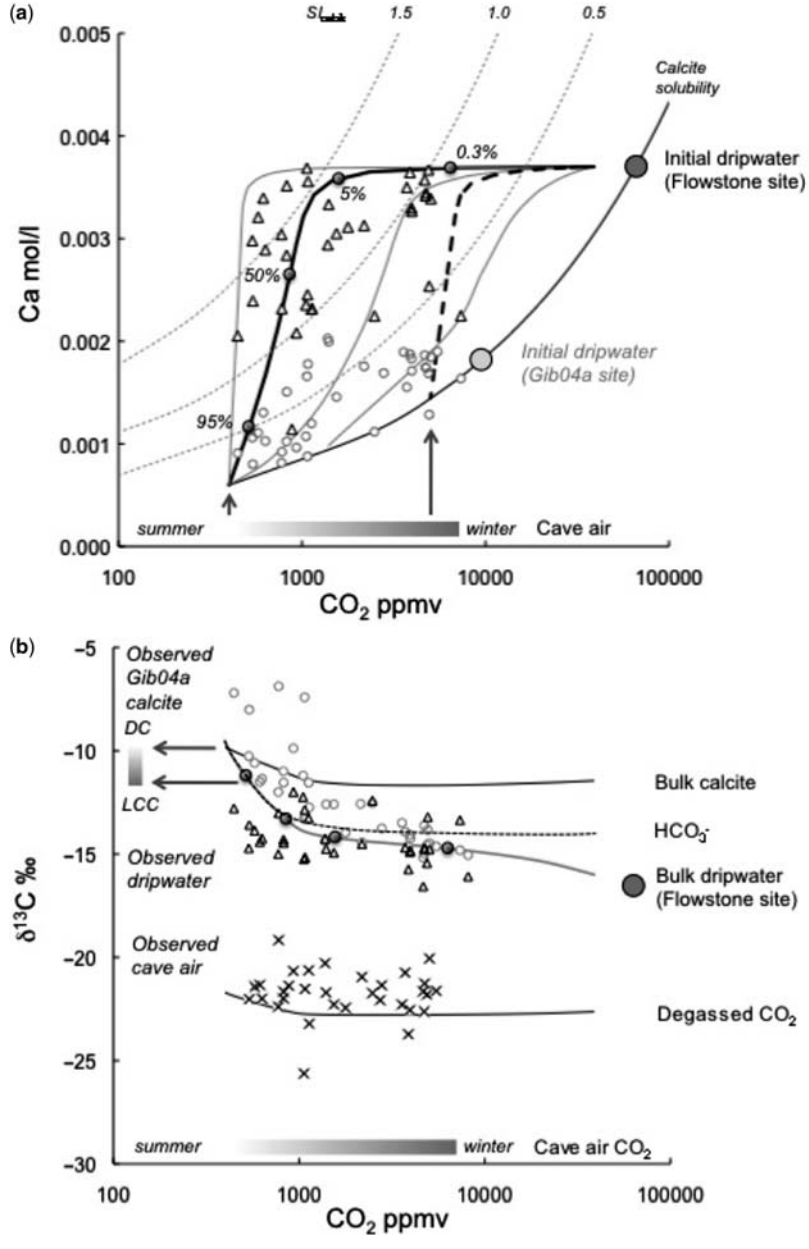

Fig. 9. Observed and modeled variations in drip water Ca and coexisting calcite, drip water and cave air $\delta^{13}C$ as a function of fluctuating cave air pCO_2 responding to seasonal reversals in cave ventilation. (**a**) Calcite solubility curve and curves representing the compositions of solutions with calcite saturation indices (log of the ratio of ionic activity product to calcite solubility product) of 0.5, 1.0 and 1.5 calculated for pure water at 18 °C using PHREEQC (Appelo & Postma 2007). The loci of solution compositions evolving via coupled degassing–calcite precipitation from an initial solution in equilibrium with calcite and air containing 70 000 ppmv CO_2 ($pCO2 \approx 10^{-1}$) containing 4.5 mmole/l Ca, of are shown for 'summer' degassing where final equilibrium would be attained under low cave air levels of ≈500 ppmv CO_2; the four curves represent cases where degassing is $\times 10$, $\times 10^2$, $\times 10^3$ (heavy line) and $\times 10^4$ greater than the rate of calcite precipitation. The cumulative amount of calcite precipitated is shown for the 10^3 curve which mirrors the evolution of dripwater at the flowstone site (triangles). The compositions of dripwater (open circles) for the Gib04a site along with a hypothetical initial solution in equilibrium with calcite and air containing 10 000 ppmv CO_2 are shown for

The two variables that exert greatest control over the solute and isotopic evolution of carbonate saturated solutions during coupled degassing–calcite precipitation are: (1) the contrast between the initial equilibrium pCO_2 and that of the new lower pCO_2 environment; and (2) the rate of CO_2 degassing relative to calcite precipitation. The contrast between the initial and final pCO_2 is well constrained by field measurements but the kinetics and rate of degassing and calcite precipitation may depend on local factors such as the discharge rate, drip size, water film thickness (for degassing) and the nucleation and crystal growth mechanisms during calcite precipitation. Figure 9a shows modeled degassing curves for the flowstone drip water compositions using an initial solution in equilibrium with pCO_2 set at 7% containing 4.5 mmol/l Ca. If the pCO_2 contrast remains small and CO_2 degassing and calcite precipitation keep pace with each other the solution will evolve following the equilibrium calcite solubility curve as pCO_2 decreases to a new lower level. For CO_2 saturated drip water emerging into a well ventilated space the CO_2 degassing rate will be much greater than the calcite precipitation rate rapidly forming calcite supersaturated solutions as shown by the drip water compositions at both the flowstone and Gib04a sites in Figure 9a.

The drip water data plotted in Figure 9a represent three complete ventilation cycles and are the end product of degassing under two regimes: winter and summer. To illustrate the effects of different degassing–calcite precipitation rates, four degassing curves are calculated for 'summer' degassing where final equilibrium would be attained under low cave air levels of ≈500ppmv CO_2. The curves represent degassing rates $\times 10$, $\times 10^2$, $\times 10^3$ and $\times 10^4$ greater than the rate of calcite precipitation and show in all cases that solutions rapidly become strongly supersaturated until delayed calcite precipitation restores equilibrium at the new lower pCO_2. As the degassing rate increases the degree of maximum supersaturation also rises and the form of these curves mirror the observed trends in drip water evolution (Fig. 9a). Flowstone drip water compositions suggest that degassing from at this site was around 10^3 times faster than calcite precipitation, and this is also the case for Gib04a drip water although at lower overall degrees of calcite supersaturation (Fig. 9a, open circles). For degassing under winter conditions the pCO_2 contrast is lower and degassing vectors will return to the equilibrium curve more quickly. This is illustrated by the dashed curve on Figure 9a which is the 10^3 rate curve (solid line) recalculated for winter degassing to a cave air pCO_2 of 5000 ppmv and embrace data at relatively low Ca levels sampled under high pCO_2 conditions on Figure 9a. Thus the spread of measured drip water compositions fit within a dynamic degassing model where degassing vectors are continuously responding not only to seasonal ventilation but possibly also to the rapid (day-week) synoptic time scale fluctuations revealed by continuous monitoring of cave air pCO_2.

The evolution of $\delta^{13}C$ in bicarbonate, cave air and calcite has been calculated as a Rayleigh model using PHREEQ as a complete system that accounts for apportionment of ^{13}C among all coexisting carbon species as a function of changing pH during degassing (Appelo & Postma 2007). Monthly values for $\delta^{13}C$ of coexisting dissolved inorganic carbon in drip water from the flowstone and Gib04a sites, and for coexisting cave air CO_2 (calculated as the end-member composition 'added' as ground air, see Fig. 8) can be compared with the modeled isotopic evolution of the composition of least degassed drip water (sampled from within roof straws at −16‰) under the same summer conditions as the solid degassing curve in Figure 9a, where the rate of CO_2 degassing is set 10^3 times faster than calcite precipitation.

Starting with an initial solution having a $\delta^{13}C$ of −16‰ (representing the bulk composition of all carbon components, measured as total DIC) measured and calculated data $\delta^{13}C_{DIC}$ are closely comparable and $\delta^{13}C_{DIC}$ values rise as a result of degassing of isotopically light carbon under decreasing cave air pCO_2. The modeled bulk isotopic composition of carbonate is initially remains fairly constant at around −12.5‰ and rises to around −10‰ during the final stages of degassing. Although the instantaneous isotopic composition of calcite will track that of dissolved bicarbonate and would rise to isotopically heavy values during the final stages of degassing, the modeled range in

Fig. 9. (*Continued*) comparison. The dashed curve represents the case where degassing takes place under winter high pCO_2 conditions. (**b**) Monthly values for $\delta^{13}C$ of dissolved inorganic carbon in drip water from the flowstone (and Gib04a) sites coexisting with end-member cave air CO_2 compared with the isotopic evolution of dripwater total DIC, dripwater HCO_3^- degassed CO_2 and precipitated calcite. The parent drip water has an initial $\delta^{13}C_{DIC}$ of −16‰ and degasses under the same summer conditions plotted in Figure 9a as the solid curve. The amplitude of calcite $\delta^{13}C$ annual cycles in Gib04a are also shown (from Fig. 10 and Mattey *et al.* 2008) which closely match the modeled evolution of calcite $\delta^{13}C$ responding to degassing. See text for discussion. [Degassing curves are calculated using PHREEQC and code adapted from Appelo & Postma (2007) with calcite precipitation rate constants from Plummer *et al.* (1978) and relevant isotope fractionation factors from Clark & Fritz (1997).]

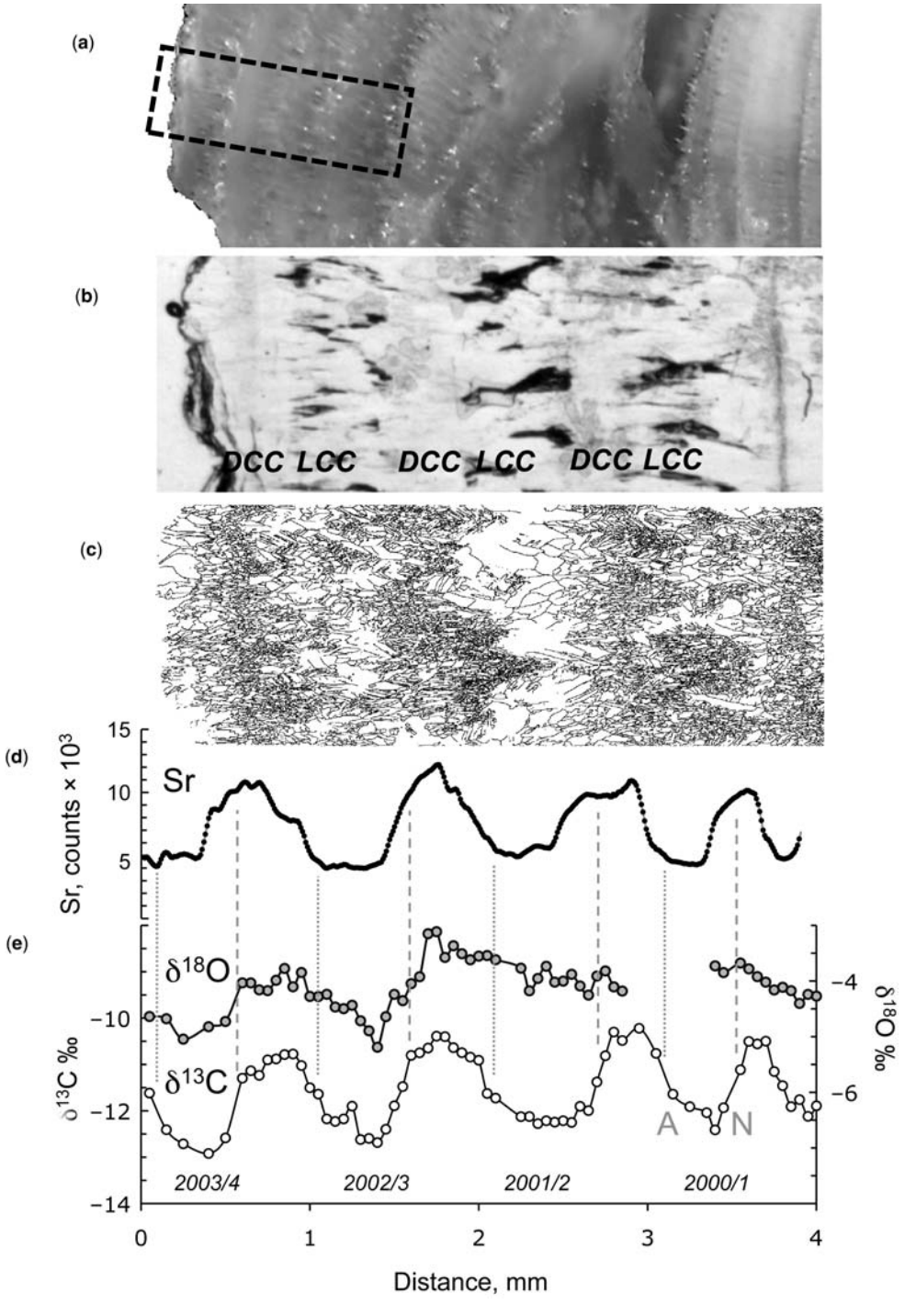

Fig. 10. Relationship between petrographic, trace element and stable isotope variations for laminae pairs growing over four years from 2000–2004 in Gib04a. (**a**) Macroscopic appearance of the uppermost portion of Gib04a. Active growth surface on left; width of image 11 mm and adapted from Mattey *et al.* (2008). (**b**) Area outlined in (a) prepared from facing slice as a thin section and viewed in plane polarized light. DCC, Dark compact calcite; LCC, light columnar

bulk calcite $\delta^{13}C$ resulting from winter–summer ventilation cycles of 2–2.5‰ is very similar in magnitude to the $\delta^{13}C$ cycles preserved in Gib04a (Mattey *et al.* 2008) and there is no evidence of kinetically enhanced $\delta^{13}C$ values as found at Obir cave by Spötl *et al.* (2005).

The isotopic composition of degassed CO_2 shows a similar pattern, the initial stages of degassing show little change around −23‰, rising only in the final stages of degassing to around −22‰. The calculated $\delta^{13}C$ trend for degassed CO_2 is only slightly lower than the $\delta^{13}C$ of end-member cave air CO_2 but a close match would only be expected if the source of cave-air CO_2 was solely from locally degassed dripwater. This cannot be the case as the quantity of drip water percolating into NSM is very low and the behaviour of CO_2 in the cave suggests that advective processes introduce 'ground air' CO_2 from elsewhere.

Paired laminae in Gib04a: relationships between cave microclimate and calcite fabric, stable isotope and trace element cycles

Modern calcite deposition in NSM results in paired laminae composed of light columnar calcite (LCC) and dark compact calcite (DCC) which preserved regular cycles in trace elements, $\delta^{13}C$ and $\delta^{18}O$ (Mattey *et al.* 2008). Mattey *et al.* (2008) assigned each lamina pair to a calendar year by counting back from the time of collection (June 2004) and the age model was confirmed by locating the radiocarbon 'bomb' peak in its correct position. The cycles in $\delta^{13}C$ and $\delta^{18}O$ reported in Mattey *et al.* (2008) were defined by samples taken at 100-μm resolution which produced quasi-regular sinusoidal variation in $\delta^{13}C$, but variations in $\delta^{18}O$ and Sr were more complex. The $\delta^{13}C$ minima were found to be located in the LCC fabric and the switch to DCC fabrics occurs when $\delta^{13}C$ and $\delta^{18}O$ are reaching highest values of the annual cycle but the precise position of the LCC-DCC fabric transition relative to stable and trace element cycles, and their timing within the annual cycle were more difficult to locate.

The cave air monitoring results shows that the switch between winter high-CO_2 and summer low-CO_2 and back again is very rapid (Fig. 7) and provide time markers for mid-April and mid-November in the annual cycle of $\delta^{13}C$ in calcite, which can be used to obtain a better understanding of environmental and kinetic controls on fabric type and trace element uptake during calcite precipitation. The correlation between paired fabrics, calcite Sr abundance, and stable isotope composition across four growth cycles – representing calcite deposited between 2000–2004 – are shown in Figure 10. Figure 10a, taken from Mattey *et al.* (2008), shows the macroscopic appearance of the uppermost portion of Gib04a in a polished surface where the paired LCC and DCC can be seen. Figures 10b and 10c show the structure of the final four cycles in plane polarized light and as an electron backscattered diffraction grain boundary map which clearly shows the alternations of columnar macroporous LCC calcite with the microporous compact DCC calcite which forms the darker bands visible on cut surfaces. The ESBD image in Figure 8c shows that the boundary surface between the LCC and DCC fabrics is irregular and is marked by a sharper transition from coarse- to fine-grained. The DCC fabric increases in grain size and the transition back to LCC is more diffuse (Fig. 8b).

A new stable isotope profile obtained by micromilling at 50-μm resolution was performed adjacent to the high resolution trace element profile by obtained by synchrotron analysis reported in Mattey *et al.* (2008) to examine the topology of the isotopic transitions between the LCC and DCC fabrics. The stable isotope, trace element and fabric maps can now be correlated with a confidence of ±100 μm.

Each analysis in the stable isotope profile in Figure 10 nominally represents 2–3 weeks of growth. They show that the cyclical pattern in $\delta^{13}C$ rises to values that remain fairly constant before falling more sharply to the lower 'winter' value. The abrupt switching of pCO_2 in the cave atmosphere implies that the annual cycle of $\delta^{13}C$ in the calcite should be a square wave. The high resolution record in Figure 10 may represent a somewhat rounded version of this, rather than the sinusoidal patterns seen in the lower resolution profile reported in Mattey *et al.* (2008). Here the rounding is introduced because the boundary surface between the LCC and DCC fabrics is irregular with amplitude of up to 500 μm. Micromill sampling in 50 μm increments along a 2 mm wide face aligned parallel to the layering of the laminae cannot fully resolve a sharp isotopic change corresponding to the jump in cave air pCO_2 that occurs in November and April.

A Sr profile across the four annual cycles was measured by synchrotron micro-XRF (Mattey

Fig. 10. (*Continued*) calcite (adapted from Mattey *et al.* (2008). (**c**) Grain boundary map of (b) obtained by electron backscatter diffraction. (**d**) Sr profile measured by synchrotron μ-XRF using a beam 1 micron across in 10 micron steps (data from Mattey *et al.* 2008). (**e**) $\delta^{13}C$ and $\delta^{18}O$ profile measured on samples removed from slab (a) in 50 micron steps by micromilling. Timelines for mid-November (N, grey dashed) and mid-April (A, grey dotted) are shown for reference. The faint dark band is radiation damage cause by synchrotron microbeam analysis. See text for discussion.

et al. 2008). The Sr/Ca ratios varies by around a factor of 2 in dripwater during the monitoring period at Gib04a (Fig. 6b) which is comparable with the range of calcite Sr in Figure 10, making it unnecessary to invoke kinetic effects to account for annual Sr variability at this site (cf. Fairchild & Treble 2009). The data in Figure 10 were obtained using a 1 micron beam in 10 micron steps. They are not affected by mixing of different calcite types caused by sampling parallel to irregular boundaries, but suffer from a different problem in that the precise position of the irregular LCC–DCC boundary cannot precisely be mapped along the Sr line traverse. However it can be seen that Sr variations closely follow the pattern of variation in $\delta^{13}C$, but Sr values are more constant during winter deposition of LCC and in summer, where $\delta^{13}C$ is more uniformly high (i.e. a plateau with rounded shoulders caused by micromill sampling), Sr values peak then gradually decline.

Time lines corresponding to mid-April and mid-November are shown on Figure 10 and it is apparent that the Sr cycle begins its rise at about the time of the April transition, but reaches a short-lived maximum well *before* the November transition in July or August. The Sr values then decline through the autumn and the minimum is reached *after* the November transition. Neither the poor 'square wave' resolution of the Micromill nor the uncertainty of the fabric boundaries with respect to Sr can influence these phase relations, which must have a different explanation. One possibility is that the timing reflects the influence of drop interval on degassing and PCP onto the straw stalactite above Gib04a. The discharge log in Figure 5 shows that discharge generally increases for a month or two in mid-summer to autumn, but because the logged years do not cover the four years of speleothem growth shown in Figure 10a precise comparison is not possible. Nevertheless, if discharge regularly increases in late summer, as it seems to, there would be less time between drops for degassing and therefore less PCP, so Sr/Ca would fall. We suggest timing of the Sr peak represents the onset of increased summer flow at Gib04a; flow is then slowly reduced again resulting in increased Sr/Ca values before the November CO_2 rise reduces degassing more completely. After the sharp winter switch in pCO_2, PCP slows down and Sr/Ca falls sharply to the winter minimum plateau.

Thus the details of the $\delta^{13}C$ and Sr cycles appear to be subtly decoupled from each other with respect to fabric development. This is consistent with the results of the degassing–calcite precipitation process modeled above in which degassing rates are highly responsive to seasonally variable cave air pCO_2 whereas calcite precipitation rates (around 10^3 slower, see above) drive the PCP enrichment of Sr at a far slower rate. Banner *et al.* (2007) also showed that calcite precipitation can temporally cease under high cave air pCO_2 conditions and the sharper junction between LCC back to DCC may represent a temporary cessation of growth, also marked by steps in Sr concentration in the calcite. Clearly, even at this resolution and high level of confidence in correlating fabrics and chemical profiles, the fabric–isotope–trace element relations still remain rather ambiguous. However the jumps in $\delta^{13}C$ clearly mark the suppression and restoration of degassing as cave air pCO_2 levels rise and fall sharply in mid-November and mid-April accompanied with synchronous changes in $\delta^{18}O$.

Because no clear evidence exists of kinetic enhancement of $\delta^{13}C$ during seasonal cycles several other processes may control the irregular annual $\delta^{18}O$ excursions to heavier values seen in Figure 10, including changes in the composition of the drip water, and will be discussed further elsewhere. The minimum $\delta^{18}O$ values, as discussed in Mattey *et al.* (2008), represent the dripwater compositions recorded when the cave environment is most conducive to equilibrium precipitation (i.e. lowest $\delta^{13}C$ and highest cave air pCO_2) and these values correlate well with the weighted mean $\delta^{18}O$ of winter precipitation over a 54-year period (Mattey *et al.* 2008).

Conclusions

Detailed monitoring of three drip sites in NSM reveals a strongly coherent seasonal pattern of dripwater compositions despite each site having significantly different flow paths and discharge patterns. Calcite saturation is closely linked to regular seasonal variations in cave air pCO_2 which is highest between November–April. The seasonal switch to low pCO_2 in the summer is caused by chimney ventilation linked to temperature differences between the exterior and interior of the cave. Advection of isotopically homogenous CO_2-rich ground air derived from deeper levels in the Rock maintains high cave air pCO_2 levels resulting in winter speleothem deposition of columnar calcite having the lowest $\delta^{13}C$ and $\delta^{18}O$ values. Flushing by the outside atmosphere lowers cave air pCO_2 levels in summer leading to higher degrees of dripwater degassing rates precipitation a dark compact calcite having elevated $\delta^{13}C$ values.

A coupled CO_2 degassing–calcite precipitation model links the development of annual cycles in $\delta^{13}C$ and dripwater evolution to switching pCO_2 driven by seasonal cave ventilation. The model shows that drip water supersaturation is consistent with degassing rates 10^4 greater than the rate of calcite precipitation and also accounts for the

observed seasonal $\delta^{13}C$ variations in coexisting dripwater, cave air CO_2 and speleothem calcite.

The relationships between stable isotope, Sr and speleothem fabrics across calcite laminae deposited between 2000 and 2004 have been examined at the highest possible resolution using micromilling, synchrotron μ-XRF and electron backscatter diffraction techniques and shows that $\delta^{13}C$ and Sr are subtly decoupled from each other with respect to fabric development. The Sr- $\delta^{13}C$ topology is consistent with a degassing–calcite precipitation process where the $\delta^{13}C$ compositions of drip water and calcite are highly responsive to seasonally switching cave air pCO_2 whereas calcite precipitation rates (up to 10^4 slower, see above) drive the PCP enrichment of Sr at a slower and more complex manner.

High resolution speleothem fabric, trace element and isotope records from caves that have been closely monitored provide crucial links between the local climate and the way that climate is recorded during speleothem deposition and remove some of the assumptions sometimes necessary in climate reconstruction from speleothem records. In Gibraltar the low cave air pCO_2 in summer is unusual compared to cave monitoring studies carried out elsewhere and shows that caution is needed when linking paired speleothem fabrics to specific seasons without knowledge of local processes operating in the cave. Furthermore, monitoring shows that the climate recording process may vary among sites in the same cave resulting in differing bias to winter and summer growth depending on the interplay between ventilation and hydrological cycles.

We are indebted to John Balestrino, Joanne McCarthy and Hela de la Paz for help with the cave monitoring program, to John Cortes (GONHS) for logistic support, and Tito Vallejo and the cave guides for their co-operation. We also thank Jacqui Duffet, Dave Lowry and Rebecca Fisher for assistance in the laboratory and field during the project. The manuscript was greatly improved with the help of comments made by two anonymous reviewers. This work was supported by the NERC under grant NE/D005280.

References

APPELO, C. A. J. & POSTMA, D. 2007. *Geochemistry, groundwater and pollution*. Balkema Publishers, Leiden, The Netherlands.

ATKINSON, T. C. 1977. Carbon dioxide in the atmosphere of the unsaturated zone: an important control of groundwater hardness in limestones. *Journal of Hydrology*, **35**, 111–123.

ATKINSON, T. C., SMART, P. L. & WIGLEY, T. M. L. 1983. Climate and natural radon levels in Castleguard Cave, Columbia Icefields, Alberta, Canada. *Arctic and Alpine Research*, **15**, 487–502.

BAKER, A. & BRUNSDON, C. 2003. Non-linearities in drip water hydrology: an example from Stump Cross Caverns, Yorkshire. *Journal of Hydrology*, **277**, 151–163.

BAKER, A., SMITH, C. L., JEX, C., FAIRCHILD, I. J., GENTY, D. & FULLER, L. 2008. Annually laminated speleothems: a review. *International Journal of Speleology*, **37**, 193–206.

BALDINI, J. U. L., MCDERMOTT, F., BAKER, A., BALDINI, L. M., MATTEY, D. P. & RAILSBACK, L. B. 2005. Biomass effects on stalagmite growth and isotope ratios: a 20th century analogue from Wiltshire, England. *Earth and Planetary Science Letters*, **240**, 486–494.

BALDINI, J. U. L., MCDERMOTT, F. & FAIRCHILD, I. J. 2006. Spatial variability in cave drip water hydrochemistry: implications for stalagmite paleoclimate records. *Chemical Geology*, **235**, 290–304.

BALDINI, J. U. L., MCDERMOTT, F., HOFFMANN, D. L., RICHARDS, D. A. & CLIPSON, N. 2008. Very high-frequency and seasonal cave atmosphere P_{CO2} variability: Implications for stalagmite growth and oxygen isotope-based paleoclimate records. *Earth and Planetary Science Letters*, **272**, 118–129.

BANNER, J. L., GUILFOYLE, A., JAMES, E. W., STERN, L. A. & MUSGROVE, M. 2007. Seasonal Variations in Modern Speleothem Calcite Growth in Central Texas, U.S.A. *Journal of Sedimentary Research*, **77**, 615–622.

BAR-MATTHEWS, M., AYALON, A., MATTHEWS, A., SASS, E. & HALICZ, L. 1996. Carbon and oxygen isotope study of the active water–carbonate system in a karstic Mediterranean cave: implications for palaeoclimate research in semiarid regions. *Geochimica et Cosmochimica Acta*, **60**, 337–347.

BORSATO, A., FRISIA, S., FAIRCHILD, I. J., SOMOGIY, A. & SUSINI, J. 2007. Trace element distribution patterns in annual stalagmite laminae mapped by micrometer-resolution X-ray fluorescence: incorporation of colloidally-transported species. *Geochimica et Cosmochimica Acta*, **71**, 1494–1512.

BOTTRELL, S. H. & ATKINSON, T. C. 1992. Tracer study of flow and storage in the unsaturated zone of a karstic limestone aquifer. *In*: HÖTZL, H. & WERNER, A. (eds) *Tracer Hydrology*. Balkema, Rotterdam, 207–211.

CLARK, I. D. & FRITZ, P. 1997. *Environmental Isotopes in Hydrogeology*. CRC Lewis Publishers, New York.

COLLISTER, C. J. & MATTEY, D. P. 2008. Controls on water drop volume at speleothem drip sites: an experimental study. *Journal of Hydrology*, **358**, 259–267.

CRUZ, F. W., KARMANN, I. *ET AL.* 2005. Stable isotope study of cave percolation waters in subtropical Brazil: Implications for paleoclimate inferences from speleothems. *Chemical Geology*, **220**, 245–252.

EK, C. & GEWELT, M. 1985. Carbon dioxide in cave atmospheres. New results in Belgium and comparison with some other countries. *Earth Surface Processes and Landforms*, **10**, 173–187.

FAIRCHILD, I. J. & TREBLE, P. C. 2009. Trace elements in speleothems as recorders of environmental change. *Quaternary Science Reviews*, **28**, 449–468.

FAIRCHILD, I. J., BORSATO, A. *ET AL.* 2000. Controls on trace element (Sr–Mg) compositions of carbonate cave waters: implications for speleothem climatic records. *Chemical Geology*, **166**, 255–269.

FAIRCHILD, I. J., SMITH, C. L. *ET AL*. 2006*a*. Modification and preservation of environmental signals in speleothems. *Earth-Science Reviews*, **75**, 105–153.

FRAPPIER, A., SAHAGIAN, D., GONZALEZ, L. A. & CARPENTER, S. J. 2002. El Niño events recorded by stalagmite carbon isotopes. *Science*, **298**, 565.

GENTY, D. & QUINIF, Y. 1996. Annually laminated sequences in the internal structure of some Belgian stalagmites – importance for paleoclimatology. *Journal of Sedimentary Research*, **66**, 275–288.

GENTY, D. & DEFLANDRE, G. 1998. Drip flow variations under a stalactite of the Père Noël cave (Belgium). Evidence of seasonal variations and air pressure constraints. *Journal of Hydrology*, **211**, 208–232.

GENTY, D., BAKER, A., MASSAULT, M., PROCTOR, C., GILMOUR, M., PONS, E. & HAMELIN, B. 2001. Stalagmite dead carbon proportion variation: paleodissolution process and soil organic matter dynamics recorder - implications for 13C variations in stalagmites. *Geochimica et Cosmochimica Acta*, **65**, 3443–3457.

GENTY, D. 2008. Palaeoclimate research in Villars Cave (Dordogne, SW-France). *International Journal of Speoleology*, **37**(3), 173–191.

HENDY, C. H. 1971. The isotopic geochemistry of speleothems - I. The calculation of the effects of different modes of formation on the isotopic composition of speleothems and their applicability as palaeoclimatic indicators. *Geochimica Cosmochimica Acta*, **35**, 801–824.

HUANG, Y. & FAIRCHILD, I. J. 2001. Partitioning of Sr^{2+} and Mg^{2+} into calcite under karst-analogue experimental conditions. *Geochimica et Cosmochimica Acta*, **65**, 47–62.

JOHNSON, K. R., HU, C., BELSHAW, N. S. & HENDERSON, G. M. 2006. Seasonal trace-element and stable isotope variations in a Chinese speleothem: the potential for high resolution paleomonsoon reconstruction. *Earth and Planetary Science Letters*, **244**, 394–407.

MATTEY, D., LOWRY, D., DUFFET, J., FISHER, R., HODGE, E. & FRISIA, S. 2008. A 53 year seasonally resolved oxygen and carbon isotope record from a modern Gibraltar speleothem: reconstructed drip water and relationship to local precipitation. *Earth and Planetary Science Letters*, **269**, 80–95.

MCDERMOTT, F. 2004. Palaeo-climate reconstruction from stable isotope variations in speleothems: a review. *Quaternary Science Reviews*, **23**, 901–918.

MICKLER, P. J., BANNER, J. L., STERN, L., ASMEROM, Y., EDWARDS, R. L. & ITO, E. 2004. Stable isotope variations in modern tropical speleothems: evaluating equilibrium vs. kinetic effects. *Geochimica et Cosmochimica Acta*, **68**, 4381–4393.

MICKLER, P. J., STERN, L. A. & BANNER, J. L. 2006. Large kinetic isotope effects in modern speleothems. *Geological Society of America Bulletin*, **118**, 65–81.

MYLROIE, J. E. & CAREW, J. L. 1988. Solution conduits as indicators of late Quaternary sea level position. *Quaternary Science Reviews*, **7**, 55–64.

PLUMMER, L. N., WIGLEY, T. M. L. & PARKHURST, D. L. 1978. The kinetics of calcite dissolution in CO_2-water systems at 5° to 60°C and 0.0 to 1.0 atm CO_2. *American Journal of Science*, **278**, 179–216.

RODRIGUEZ-VIDAL, J., CÁCERES, L. M., FINLAYSON, J. C., GRACIA, F. J. & MARTÍINEZ-AGUIRRE, A. 2004. Neotectonics and shoreline history of the Rock of Gibraltar, southern Iberia. *Quaternary Science Reviews*, **23**, 2017–2029.

ROMANOV, D. & DREYBRODT, W. 2006. Evolution of porosity in the saltwater–freshwater mixing zone of coastal carbonate aquifers: an alternative modelling approach. *Journal of Hydrology*, **329**, 661–673.

ROSE, E. P. F. & ROSENBAUM, M. S. 1991. *A field guide to the geology of Gibraltar*. The Gibraltar Museum, Bomb House Lane, Gibraltar.

ROSENBAUM, M. S. & ROSE, E. P. F. 1991. *Map: The Geology of Gibraltar*. The Gibraltar Museum, Bomb House Lane, Gibraltar.

SHAW, T. R. 1954. New St. Michaels Cave. *Cave Science*, **3**, No. 22.

SHAW, T. R. 1955. Old St. Michaels Cave. *Cave Science*, **3**, No. 24.

SMART, P. L. 1976. The use of optical brighteners for water tracing. *Transactions British Cave Research Association*, **3**(2), 62–76.

SPÖTL, C., FAIRCHILD, I. J. & TOOTH, A. F. 2005. Cave air control on dripwater geochemistry, Obir caves (Austria): implications for speleothem deposition in dynamically ventilated caves. *Geochimica et Cosmochimica Acta*, **69**, 2451–2468.

TAN, M., BAKER, A., GENTY, D., SMITH, C., ESPER, J. & CAI, B. 2006. Applications of stalagmite laminae to paleoclimate reconstructions: comparison with dendrochronology/climatology. *Quaternary Science Reviews*, **25**, 2103–2117.

THORNTHWAITE, C. W. 1948. An approach toward a rational classification of climate. *Geographic Review*, **38**, 55–94.

TOOTH, A. F. & FAIRCHILD, I. J. 2003. Soil and karst aquifer hydrological controls on the geochemical evolution of speleothem-forming drip waters, Crag Cave, southwest Ireland. *Journal of Hydrology*, **273**, 51–68.

TRATMAN, E. K. 1971. The formation of the Gibraltar Caves. *Trans Cave research Group of Great Britain*, **13**, 135–143.

TREBLE, P., SHELLEY, J. M. G. & CHAPPELL, J. 2003. Comparison of high resolution sub-annual records of trace elements in a modern (1911–1992) speleothem with instrumental cliate data from southwest Australia. *Earth and Planetary Science Letters*, **216**, 141–153.

WANG, Y., CHENG, H. *ET AL*. 2008. Millennial- and orbital-scale changes in the East Asian monsoon over the past 224,000 years. *Nature*, **451**, 1090–1093.

WIGLEY, T. M. L. & BROWN, M. C. 1976. The Physics of Caves. Ch. 9, p. 329–358. *In*: FORD, T. D. & CULLINGFORD, C. H. D. (eds) *The Science of Speleology*. Academic Press, London.

WOOD, W. W. & PETRAITIS, M. J. 1984. Origin and distribution of carbon dioxide in the unsaturated zone of the southern High Plains. *Water Resources Research*, **20**, 1193–1208.

WOOD, W. W. 1985. Origin of caves and other solution openings in the unsaturated (vadose) zone of carbonate rocks: A model for CO_2 generation. *Geology*, **13**, 822–824.